MIMO-OFDM Over An Underwater Acoustic Channel

Baosheng Li[1], Shengli Zhou[1], Milica Stojanovic[2], Lee Freitag[3], Jie Huang[1], Peter Willett[1]

[1]Dept. of Elec. and Computer Engr., University of Connecticut, Storrs, CT 06269
[2]Massachusetts Institute of Technology, Cambridge, MA 02139
[3]Woods Hole Oceanographic Institution, Woods Hole, MA 02543

Abstract— **Multicarrier modulation in the form of OFDM facilitates high-rate transmission over long dispersive channels, while multiple-input multiple-output (MIMO) techniques increase the system capacity. In this paper, we report on the design of a MIMO-OFDM with two transmitters and test it using experimental data recorded during the AUV Fest, Panama City, FL, June 2007. Nearly error-free performance is observed with low-density parity-check (LDPC) coding. With a 12 kHz bandwidth, the overall data rate is 12.18 kbps after rate 1/2 coding.**

I. Introduction

Recently, multicarrier modulation in the form of orthogonal frequency division multiplexing (OFDM) has been actively pursued for underwater acoustic (UWA) communications; see e.g., [1]–[5]. On the other front, multi-input multi-output (MIMO) techniques have been applied to UWA communications via spatial modulations [6], [7]. These MIMO approaches have leveraged existing adaptive channel equalization algorithms for single carrier transmissions [6], [7].

Due to OFDM's unique strength in handling high-speed transmissions over long dispersive channels with low equalization complexity, the combination of MIMO and OFDM leads to an appealing solution for high data rate transmissions but with low and controllable receiver complexity. Although the concept of MIMO-OFDM for UWA communications has been proposed in e.g., [8], experiment results have not been reported in the literature so far.

Building upon our single-transmitter OFDM system in [4], [5], we design a MIMO-OFDM scheme where two independent data streams are transmitted through two transmitters simultaneously. The transceiver design consists of the following key approaches:

- Null subcarriers are inserted at the transmitter to facilitate the estimation and compensation of Doppler shifts at the receiver.
- Pilot tones are used for MIMO channel estimation.
- A maximum a posteriori (MAP) or linear zero-forcing (ZF) detector is used for MIMO demodulation on each OFDM subcarrier.

- Either convolutional coding (CC) or low-density parity-check (LDPC) coding [9] is applied for reliable communication; in this paper we report on both.

As in [4], [5], our receiver design is based on block-by-block processing, which does not rely on channel coherence across OFDM blocks and is thus robust to fast channel variations across blocks.

We test the MIMO-OFDM transmission using experimental data from the AUV Fest, Panama City, FL, June 2007. Decent bit-error-rate performance is achieved with convolutional coding, while nearly error-free performance is achieved with LDPC coding. The results in this paper demonstrate the potential of MIMO-OFDM: with a 12 kHz bandwidth, the achieved raw data rate is 24.36 kbps, which doubles the raw data rate of our single-transmitter OFDM system in [5], and the overall data rate is 12.18 kbps after rate 1/2 coding.

The rest of the paper is organized as follows. The transmitter design is presented in Section II, and the receiver algorithms are developed in Section III. In Section IV we report on the performance results, and in Section V we draw conclusions.

II. Transmitter Design

We consider a MIMO-OFDM transmission with two transmitters. Within each OFDM block, two independent data streams are encoded with either a convolutional code or an LDPC code. The coded bits are mapped into information symbols using QPSK modulation; bits are also interleaved before modulation if convolutional code is used. Two OFDM blocks are formed from the two streams of information sequences and transmitted through two transmitters simultaneously. On each transmitter, we use the zero-padded (ZP) OFDM format as in

TABLE I
ZP-OFDM Parameters

Signal bandwidth	$B = 12$ kHz
OFDM block duration	$T = 81.92$ ms
Guard interval	$T_g = 25$ ms
Subcarrier spacing	$\Delta f = 11.72$ Hz
Number of subcarriers	$K = 1024$
Number of data carriers	$K_d = 672$
Number of pilot carriers	$K_p = K/4 = 256$
Number of null subcarriers	$K_n = 96$

[5]. The key transmission parameters are in Table I, while the detailed descriptions are available in [5].

With QPSK modulation and parallel data streams from two transmitters, the uncoded data rate is

$$R_{\text{uncoded}} = \frac{2 \times 2 \times K_d}{T + T_g} = 24.36 \text{ kbps} \qquad (1)$$

over the 12 kHz bandwidth, where K_d is the number of data carriers, T is the OFDM block duration, and T_g is the guard time. For coding, we use a 16-state rate 1/2 convolutional code with the generator polynomial (23,35), and a rate 1/2 regular LDPC cycle code over Galois Field GF(64) with $(n,k) = (1344, 672)$ bits [10]. With rate 1/2 coding, the overall data rate is

$$R_{\text{coded}} = \frac{1}{2} R_{\text{uncoded}} = 12.18 \text{ kbps}. \qquad (2)$$

In our transmission, each data burst consists of two packets, one with CC and the other with LDPC coding, as shown in Fig. 1. Each data packet consists of 64 OFDM blocks with a preamble inserted for synchronization.
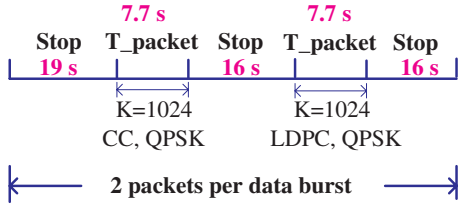

Fig. 1. The data burst structure.

III. RECEIVER ALGORITHMS

The data burst of Fig. 1 was transmitted multiple times from different locations during the AUV Fest experiment. Since performance results with four hydrophones will be presented in Section IV, here we use four receiving-elements to describe the receiver algorithms.

The transmitters and the receivers were stationary. No resampling operation as described in [5] is needed for non-uniform Doppler compensation in this experimental data set. The key processing steps are as follows.

A. Doppler estimation

The channel Doppler effect can be viewed as caused by carrier frequency offsets (CFO) among the transmitters and the receivers [4], [5]. On each receiver, we assume a common CFO relative to all transmitters, as in [11, Chapter 11.5]. Hence, the CFO estimation algorithm in Section IV.B of [5] is directly applicable, where the energy on the null subcarriers is used as the objective function to search for the best CFO estimate.

The noise variance is computed as the average energy on the null subcarriers, after CFO estimation and compensation, This quantity is needed for deriving soft bit information in the demodulation step in Section III-C.

B. Channel estimation

After CFO compensation, we use pilot tones for channel estimation. Note that at each receive antenna ν, two channels $\mathbf{h}_{\nu,1} := [h_{\nu,1}(0), \ldots, h_{\nu,1}(L)]^T$ and $\mathbf{h}_{\nu,2} := [h_{\nu,2}(0), \ldots, h_{\nu,2}(L)]^T$ need to be estimated, where L is the channel order. We divide pilot tones into two non-overlapping groups, with each group containing a set of equally-spaced subcarriers as in [11, Chapter 11]. Each group is exclusively used by one transmitter, as such channel estimation is carried out for $\mathbf{h}_{\nu,1}$ and $\mathbf{h}_{\nu,2}$ separately. Equally-spaced pilot tones can greatly simplify the complexity of the least-square (LS) channel estimator, as described in [4].

Once the channel estimates $\hat{\mathbf{h}}_{\nu,\mu}$, $\mu = 1, 2$, are available, the channel frequency response on each data subcarrier p is evaluated as

$$\hat{H}_{\nu,\mu}[p] = \sum_{l=0}^{L} \hat{h}_{\nu,\mu}(l) e^{-j2\pi pl/K}. \qquad (3)$$

Since $K_p/2 = 128$ pilots tones are used for each channel estimation, our transceiver design can only handle channels with at most $L + 1 = 128$ taps. This corresponds to a channel delay spread of 10.7 ms with $B = 12$ kHz.

C. MIMO demodulation

On each data subcarrier p, we stack the data from four receiving-elements as

$$\underbrace{\begin{pmatrix} y_1[p] \\ y_2[p] \\ y_3[p] \\ y_4[p] \end{pmatrix}}_{:=\mathbf{y}[p]} = \underbrace{\begin{pmatrix} \hat{H}_{1,1}[p] & \hat{H}_{1,2}[p] \\ \hat{H}_{2,1}[p] & \hat{H}_{2,2}[p] \\ \hat{H}_{3,1}[p] & \hat{H}_{3,2}[p] \\ \hat{H}_{4,1}[p] & \hat{H}_{4,2}[p] \end{pmatrix}}_{:=\hat{\mathbf{H}}[p]} \underbrace{\begin{pmatrix} s_1[p] \\ s_2[p] \end{pmatrix}}_{:=\mathbf{s}[p]} + \underbrace{\begin{pmatrix} n_1[p] \\ n_2[p] \\ n_3[p] \\ n_4[p] \end{pmatrix}}_{:=\mathbf{n}[p]}, \qquad (4)$$

where the noise vector is assumed Gaussian with a covariance matrix

$$\mathbf{R} = \text{diag}(\sigma_1^2, \ldots, \sigma_4^2). \qquad (5)$$

The noise variance estimation was addressed in Section III-A.

For notational convenience, we omit the subcarrier index p, and describe the detectors based on the following model

$$\mathbf{y} = \hat{\mathbf{H}}\mathbf{s} + \mathbf{n}, \qquad (6)$$

where

$$s_1 = d_1 + jd_2, \ s_2 = d_3 + jd_4, \quad d_i \in \{+1, -1\}. \qquad (7)$$

We will test two MIMO detectors, one is the optimal maximum a-posteriori (MAP) detector, and the other is the linear zero-forcing (ZF) detector.

For the MAP detector, we need to find the bit log-likelihood-ratio (LLR) defined as

$$\text{LLR}(d_i) = \ln \frac{P(d_i = 1|\mathbf{y})}{P(d_i = -1|\mathbf{y})}, \quad i = 1, \ldots, 4. \qquad (8)$$
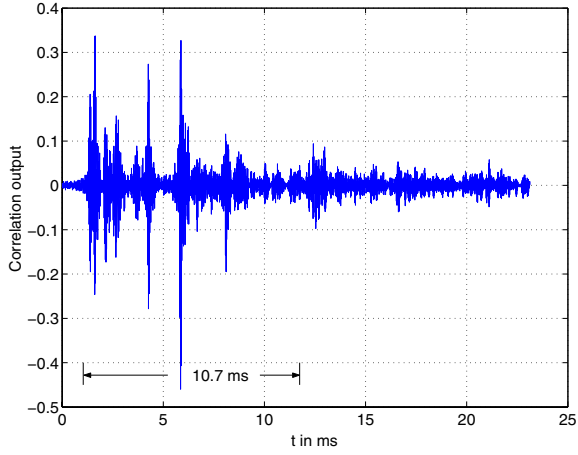
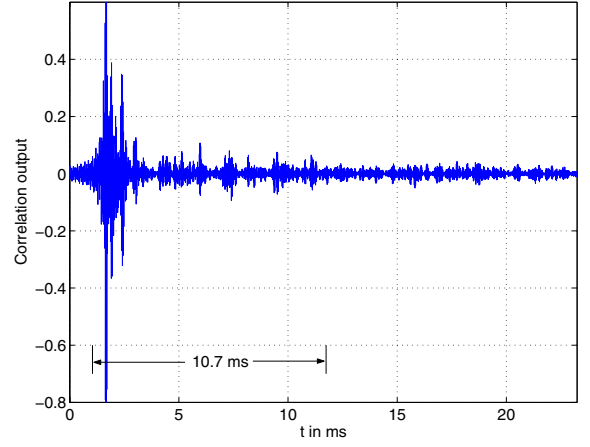Fig. 2. The channel profile based on preamble correlation, 500 m.

Fig. 3. The channel profile based on preamble correlation, 1500 m.

Fig. 4. Doppler estimates for one packet of 64 OFDM blocks at receiver 1; this Doppler shift is due to water motion.

Assuming equal prior probability $P(d_i = 1) = 1/2$ on each bit, we have

$$
\begin{aligned}
\text{LLR}(d_i) &= \ln \frac{P(\mathbf{y}|d_i = 1)}{P(\mathbf{y}|d_i = -1)} \\
&= \ln \frac{\Sigma_{\mathbf{s};d_i=1} P(\mathbf{y}|\mathbf{s})}{\Sigma_{\mathbf{s};d_i=-1} P(\mathbf{y}|\mathbf{s})} \\
&= \ln \frac{\Sigma_{\mathbf{s};d_i=1} \exp[-\|\mathbf{R}^{-\frac{1}{2}}(\mathbf{y} - \hat{\mathbf{H}}\mathbf{s})\|^2]}{\Sigma_{\mathbf{s};d_i=-1} \exp[-\|\mathbf{R}^{-\frac{1}{2}}(\mathbf{y} - \hat{\mathbf{H}}\mathbf{s})\|^2]}.
\end{aligned} \tag{9}
$$

A total of 16 possible values of the term $\exp[-\|\mathbf{R}^{-\frac{1}{2}}(\mathbf{y} - \hat{\mathbf{H}}\mathbf{s})\|^2]$ corresponding to the 16 possible values of $\mathbf{s}$ are needed to compute the LLRs for all bits.

For the ZF option, we need the pseudo-inverse of $\hat{\mathbf{H}}$ as

$$
\mathbf{A} = \hat{\mathbf{H}}^{\dagger} = (\hat{\mathbf{H}}^H \hat{\mathbf{H}})^{-1} \hat{\mathbf{H}}^H, \tag{10}
$$

where $(\cdot)^H$ denotes Hermitian transpose. The processed signal after ZF demodulation is

$$
\mathbf{z} = \mathbf{A}\mathbf{y} = \mathbf{s} + \mathbf{A}\mathbf{n}. \tag{11}
$$

Let z_1 and z_2 be the first and second entries of $\mathbf{z}$. Let t_{11}^2 and t_{22}^2 be the $(1, 1)$ and $(2, 2)$ entries of $\mathbf{A}\mathbf{R}\mathbf{A}^H$. Treating each bit as if it passes through an equivalent additive-white-Gaussian-noise (AWGN) channel, we obtain the LLR for each bit as

$$
\text{LLR}(d_1) = \frac{4\Re(z_1)}{t_{11}^2}, \qquad \text{LLR}(d_2) = \frac{4\Im(z_1)}{t_{11}^2} \tag{12}
$$

$$
\text{LLR}(d_3) = \frac{4\Re(z_2)}{t_{22}^2}, \qquad \text{LLR}(d_4) = \frac{4\Im(z_2)}{t_{22}^2}, \tag{13}
$$

where $\Re(\cdot)$ and $\Im(\cdot)$ stand for the real and imaginary parts of a complex number, respectively.

A hard decision on each bit can be obtained as

$$
\hat{d}_i = \text{sign}(\text{LLR}(d_i)). \tag{14}
$$

This is useful for the evaluation of uncoded bit error rate. The soft LLR information on each bit is passed to the channel decoder.
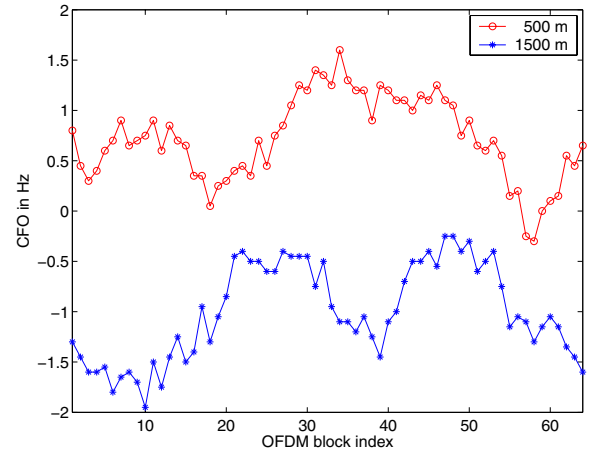
D. Decoding

For the convolutional code, we use the Viterbi algorithm for decoding. For the non-binary regular LDPC cycle code, we use the min-sum algorithm of [12] for decoding.

IV. EXPERIMENTAL RESULTS

The experimental data was collected during the AUV Fest held in Panama City, FL, June 2007. The water depth was 20 meters. The transmitter was about 9 meters below a surface buoy. The receiving array was about 9 meters below a boat. The array was 2 m in aperture with 16 hydrophones, where we only use four of them for decoding. The center frequency used was $f_c = 32$ kHz, and the signal occupied the band between 26 kHz and 38 kHz. The sampling rate was 96 kHz.

In this experiment, we tested different transmission distances of 500, 1000, 1500, and 2000 meters. We here report on the performance results for the cases of 500 and 1500 meters.

A. Channel profiles via preamble correlation

A linearly-frequency-modulated (LFM) signal is used as preamble for synchronization. The correlation results are
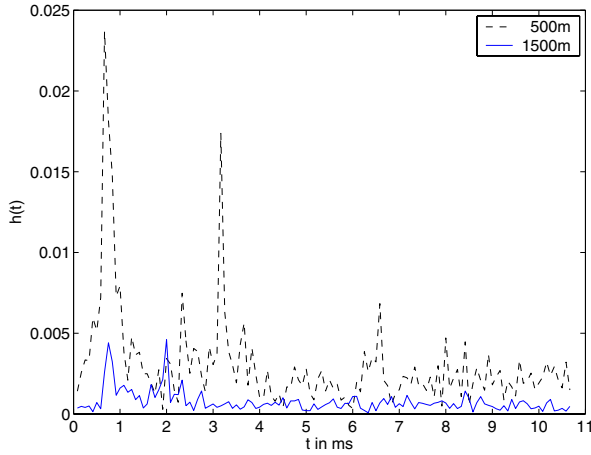
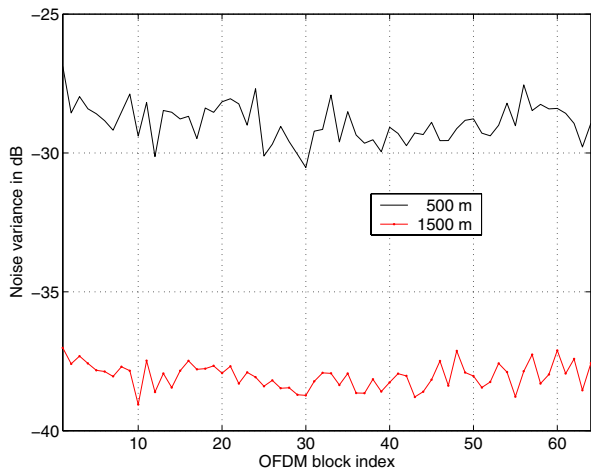Fig. 5. The estimated channel for one OFDM block on receiver 1.

Fig. 6. The average noise variance on null subcarriers for one packet.

Fig. 7. Average SNR before MIMO demodulation on receiver 1.
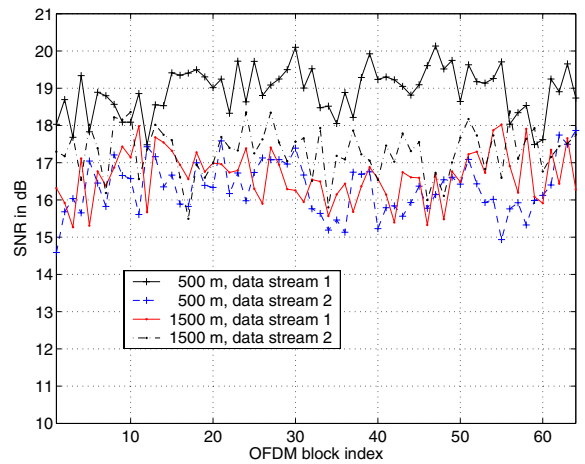
Fig. 8. Average SNR after ZF demodulation over four receivers.

shown in Fig. 2 for the 500 m case, and in Fig. 3 for the 1500 m case. It can be seen that the channel at 500 m has a larger delay spread than the channel at 1500 m, as expected.

B. CFO, Channel, and SNR estimations

The CFO estimates are shown in Fig. 4 for one data packet on one receiver. The CFO is within [-2, 2] Hz range, which is caused by transmitter and receiver drifting with waves.

The estimated channel for one OFDM block is shown in Fig. 5, which is in good agreement with the channel profiles shown in Figs. 2 and 3. It can be seen that the channel for the 500 m case is stronger. With $K_p/2 = 128$ subcarriers for each channel estimation, we can estimate 128 channel taps in discrete time, which amounts to a delay spread of 10.7 ms. Any arrivals after 10.7 ms will be treated as additive noise. Since the channel at 500 m has significant arrivals after 10.7 ms, the noise floor is much higher (around 8 dB) than that at 1500 m, as shown in Fig. 6. As a result, although the channel at 500 m is stronger than the channel at 1500 m, the pre-demodulation signal to noise ratios (SNRs) become
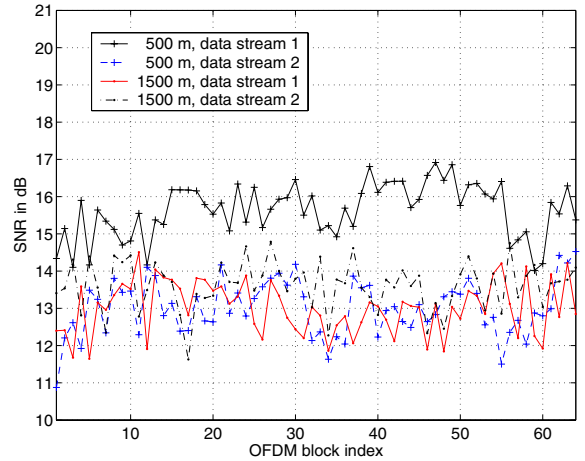
quite similar for both cases, as shown in Fig. 7; the pre-demodulation SNR is computed as the ratio of the average signal energy on the pilot subcarriers to the average energy on the null subcarriers. Also, we can see that data stream 2 has a consistently lower SNR than data stream 1 in the 500 m case. The reason for this SNR imbalance is unclear to us. However, this SNR imbalance leads to a worse BER performance in the 500 m case than that in the 1500 m case, as will be shown in Section IV-C.

In Fig. 8, we show the estimated SNR after ZF demodulation based on the channel input-output relationship in (11). These SNRs are good indicators for uncoded BER estimates presented in Section IV-C.

C. BER results

We now report on the BER results for different settings.

- *Case 1: 500 m, convolutional coding*. Figs. 9 and 10 show the BERs for data streams 1 and 2, respectively. No block has decoding errors for data stream 1, while many blocks have decoding errors for data stream 2. This is due to the SNR imbalance between these two data streams.
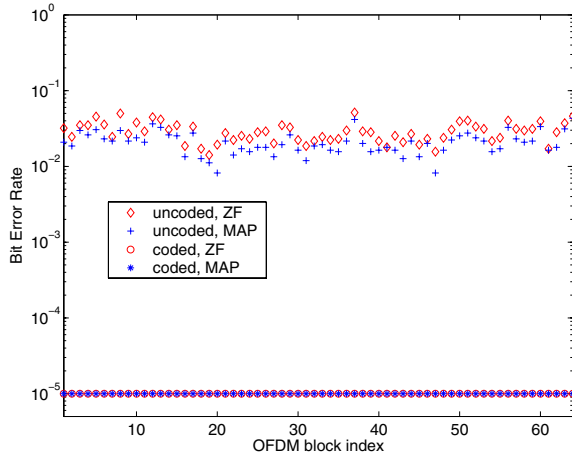
Fig. 9. The 500 m case, data stream 1, convolutional coding; BER=0 is plotted in the figure as BER=1e-5 for visualization; no block has decoding errors.
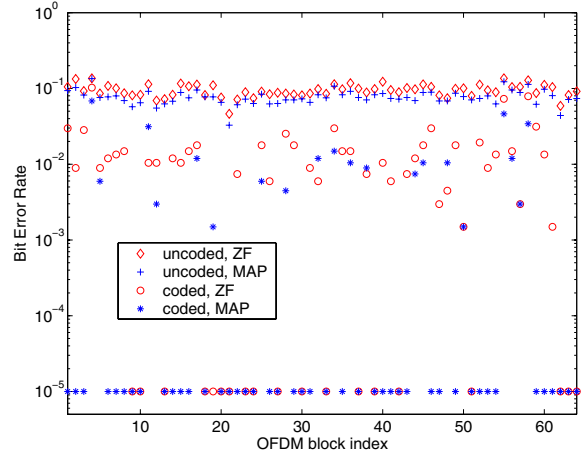

Fig. 10. The 500 m case, data stream 2, convolutional coding; BER=0 is plotted in the figure as BER=1e-5 for visualization; 44 and 33 out of 64 blocks have decoding errors after ZF and MAP equalization, respectively.
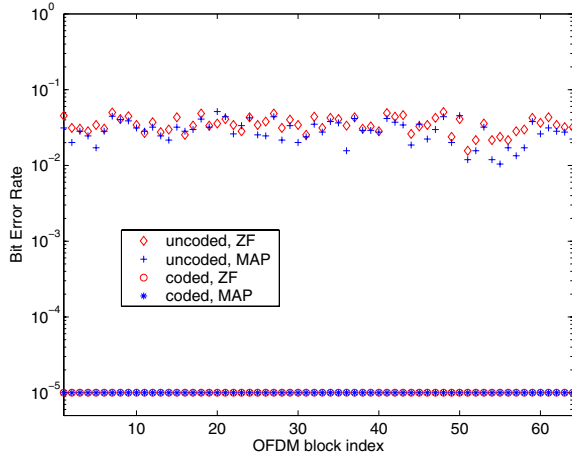

Fig. 11. The 500 m case, data stream 1, LDPC coding; BER=0 is plotted in the figure as BER=1e-5 for visualization; no block has decoding errors.
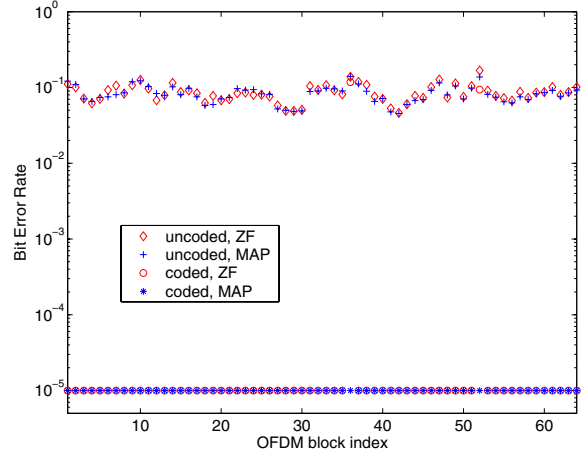

Fig. 12. The 500 m case, data stream 2, LDPC coding; BER=0 is plotted in the figure as BER=1e-5 for visualization; 2 and 0 out of 64 blocks have decoding errors after ZF and MAP equalization, respectively.
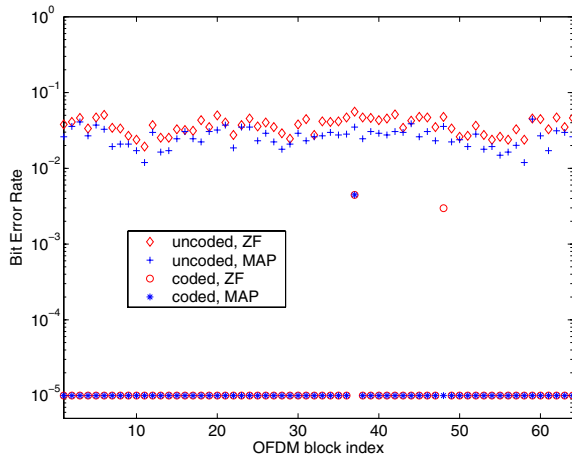

Fig. 13. The 1500 m case, data stream 1, convolutional coding; BER=0 is plotted in the figure as BER=1e-5 for visualization; 2 and 1 out of 64 blocks have decoding errors after ZF and MAP equalization, respectively.
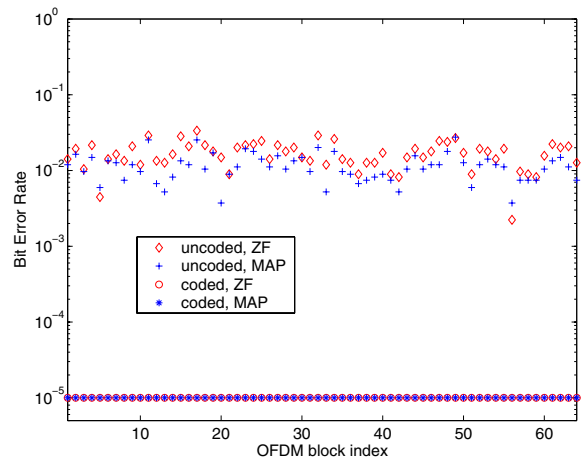

Fig. 14. The 1500 m case, data stream 2, convolutional coding; BER=0 is plotted in the figure as BER=1e-5 for visualization; no block has decoding errors.

- *Case 2: 500 m, LDPC coding*. Figs. 11 and 12 show the BERs for data streams 1 and 2, respectively. Only two out of 64 blocks have decoding errors for data stream 2 when ZF equalizer is used. All other cases have no decoding errors. The LDPC code used here has much stronger error-correcting capability than the convolutional code. When decoding, the maximum number of iterations is set as 80. The average number of iterations, however, is around 4.

- *Case 3: 1500 m, convolutional coding*. Figs. 13 and 14 show the BERs for data streams 1 and 2, respectively. The BER performance of the 1500 m case is better than that of the 500 m case, due to the much balanced SNRs between the two data streams, as shown in Fig. 8.

- *Case 4: 1500 m, LDPC coding*. Similar uncoded BERs are found as those of the convolutional coding case at 1500 m. There is no error after LDPC decoding.

We observe that: 1) the uncoded BER performance of the MAP detector is slightly better than that of the ZF detector; 2) Coding improves the BER performance drastically; and 3) the adopted regular LDPC cycle code over GF(64) is very powerful: out of all cases tested, only 2 blocks are in error in the 500 m case for data stream 2 with ZF equalization. Whenever the uncoded BER is below 0.1, all errors are corrected after LDPC decoding.

If desired, iterative receivers can be developed for further performance improvement, where the soft bit information from the channel decoder is fed back to the MIMO MAP detector as prior probability on the bits to be detected.

V. Conclusions

In this paper, we presented performance results of a MIMO-OFDM system with two transmitters and four receivers, based on experimental data from AUV Fest 2007. Excellent BER performance is achieved with channel coding. This experiment demonstrates the potential of MIMO-OFDM: with a 12 kHz bandwidth, the achieved data rate without coding is 24.36 kbps, which doubles that of our single-transmitter OFDM system in [5], and the overall data rate is 12.18 kbps after rate 1/2 coding. In our future work, we would like to investigate MIMO-OFDM systems that can handle more than two transmitters for further rate increase.

REFERENCES

[1] M. Chitre, S. H. Ong, and J. Potter, "Performance of coded OFDM in very shallow water channels and snapping shrimp noise," in *Proceedings of MTS/IEEE OCEANS*, vol. 2, 2005, pp. 996–1001.

[2] P. J. Gendron, "Orthogonal frequency division multiplexing with on-off keying: Noncoherent performance bounds, receiver design and experimental results," *U.S. Navy Journal of Underwater Acoustics*, vol. 56, no. 2, pp. 267–300, Apr. 2006.

[3] M. Stojanovic, "Low complexity OFDM detector for underwater channels," in *Proc. of MTS/IEEE OCEANS conference*, Boston, MA, Sept. 18-21, 2006.

[4] B. Li, S. Zhou, M. Stojanovic, and L. Freitag, "Pilot-tone based ZP-OFDM demodulation for an underwater acoustic channel," in *Proc. of MTS/IEEE OCEANS conference*, Boston, MA, Sept. 18-21, 2006.

[5] B. Li, S. Zhou, M. Stojanovic, L. Freitag, and P. Willett, "Non-uniform Doppler compensation for zero-padded OFDM over fast-varying underwater acoustic channels," in *Proc. of MTS/IEEE OCEANS conference*, Aberdeen, Scotland, June 18-21, 2007.

[6] D. B. Kilfoyle, J. C. Preisig, and A. B. Baggeroer, "Spatial modulation experiments in the underwater acoustic channel," *IEEE Journal of Oceanic Engineering*, vol. 30, no. 2, pp. 406–415, Apr. 2005.

[7] S. Roy, T. M. Duman, V. McDonald, and J. G. Proakis, "High rate communication for underwater acoustic channels using multiple transmitters and space-time coding: Receiver structures and experimental results," *IEEE Journal of Oceanic Engineering*, Feb. 2007.

[8] R. F. Ormondroyd, "A robust underwater acoustic communication system using OFDM-MIMO," in *Proc. of MTS/IEEE OCEANS conference*, Aberdeen, Scotland, June 18-21, 2007.

[9] R. G. Gallager, *Low Density Parity Check Codes,* Cambridge, MA: MIT Press, 1963.

[10] J. Huang, S. Zhou, and P. Willett, "On regular LDPC cycle codes over GF(q)," *IEEE Transactions on Information Theory*, in preparation.

[11] G. B. Giannakis, Z. Liu, X. Ma, and S. Zhou, *Space-Time Coding for Broadband Wireless Communications*, John Wiley & Sons, Dec. 2006.

[12] H. Wymeersch, H. Steendam, and M. Moeneclaey, "Log-domain decoding of LDPC codes over GF(q)," in Proc. IEEE International Conference on Communications, pp. 772-776, 2004.